Supplementary Information for

Nanoscale light-matter interactions in metal-organic frameworks cladding optical fibers

Jieyun Wu*, Wanying Zhang, Ying Wang*, Binghui Li, Ting Hao, Youbin Zheng, Lianzhong Jiang, Kaixin Chen, Kin Seng Chiang*

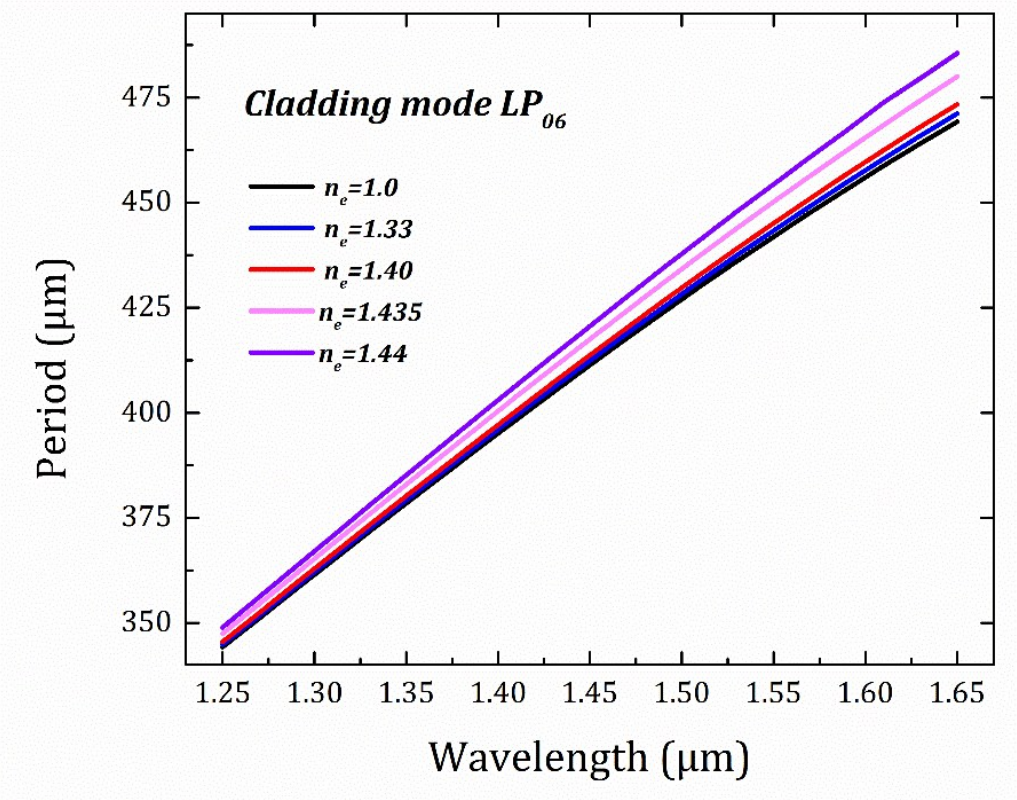

Figure S1. Simulation of cladding mode LP_{06} for refractive index sensing.

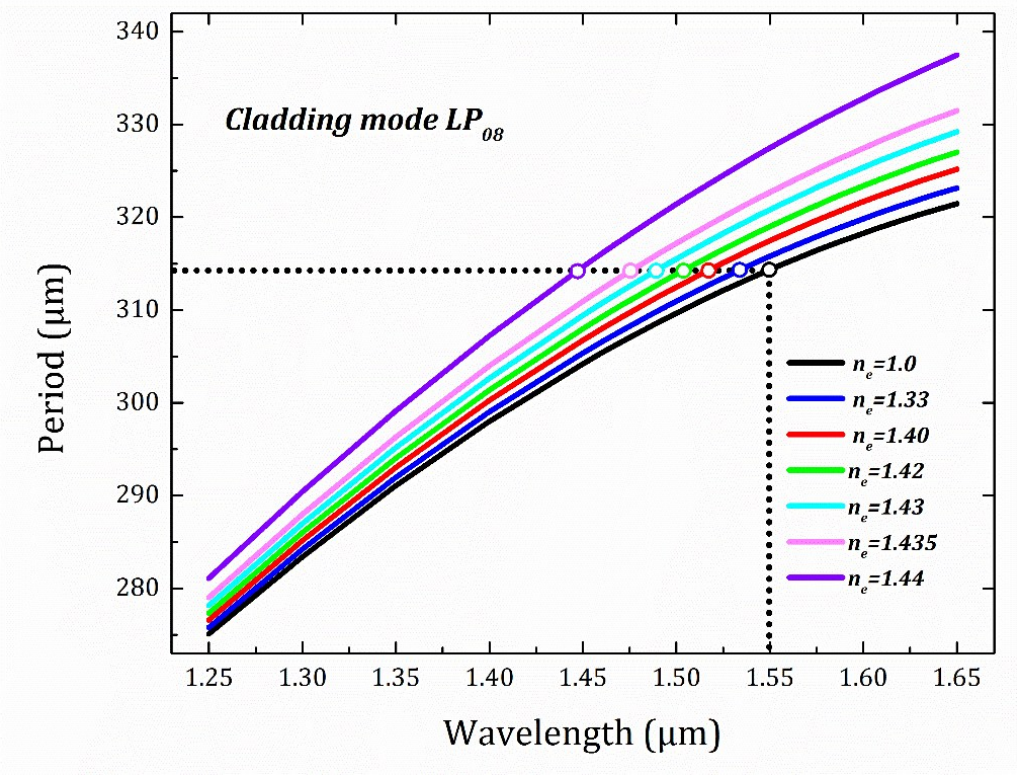

Figure S2. Simulation of cladding mode LP_{08} for refractive index sensing.

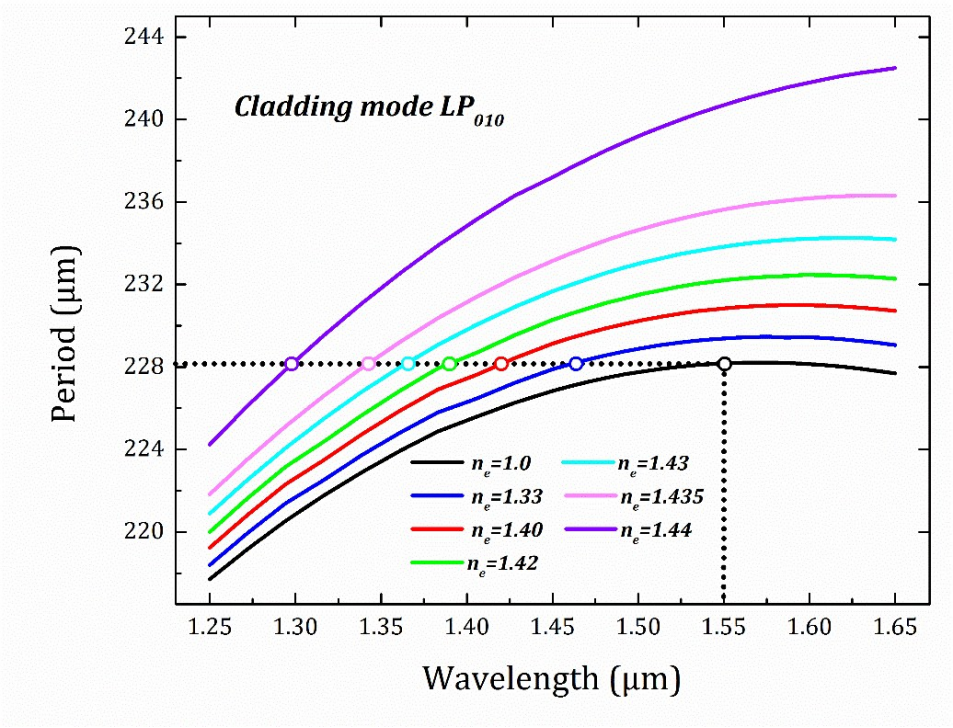

Figure S3. Simulation of cladding mode LP_{10} for refractive index sensing.

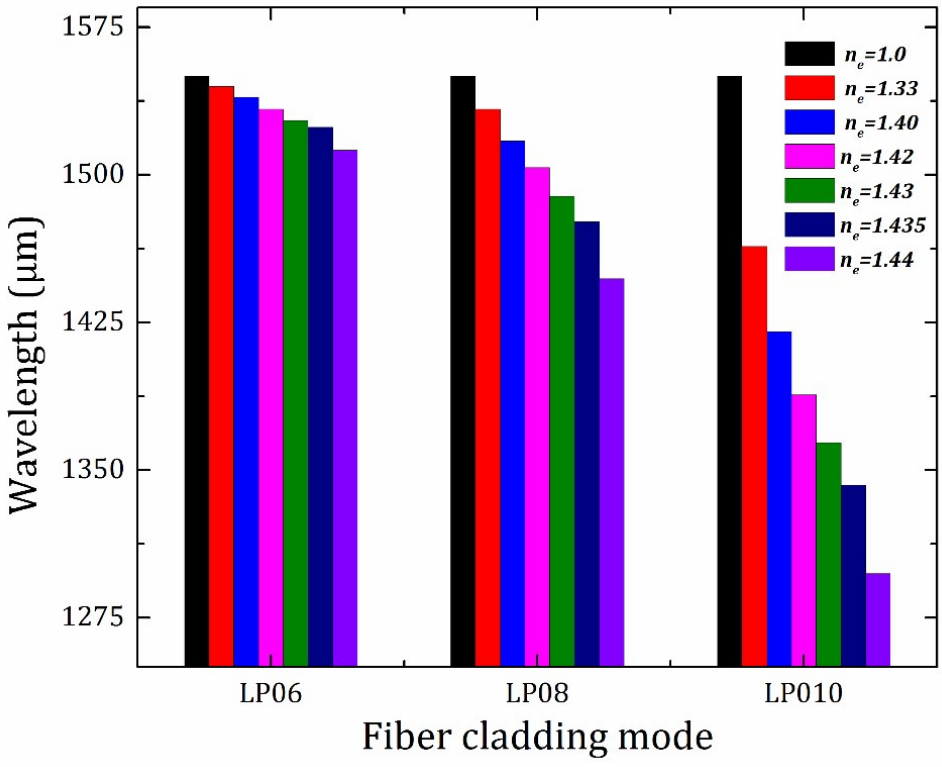

Figure S4. Comparison of central wavelength shift of LPFG in response to external refractive index changes.

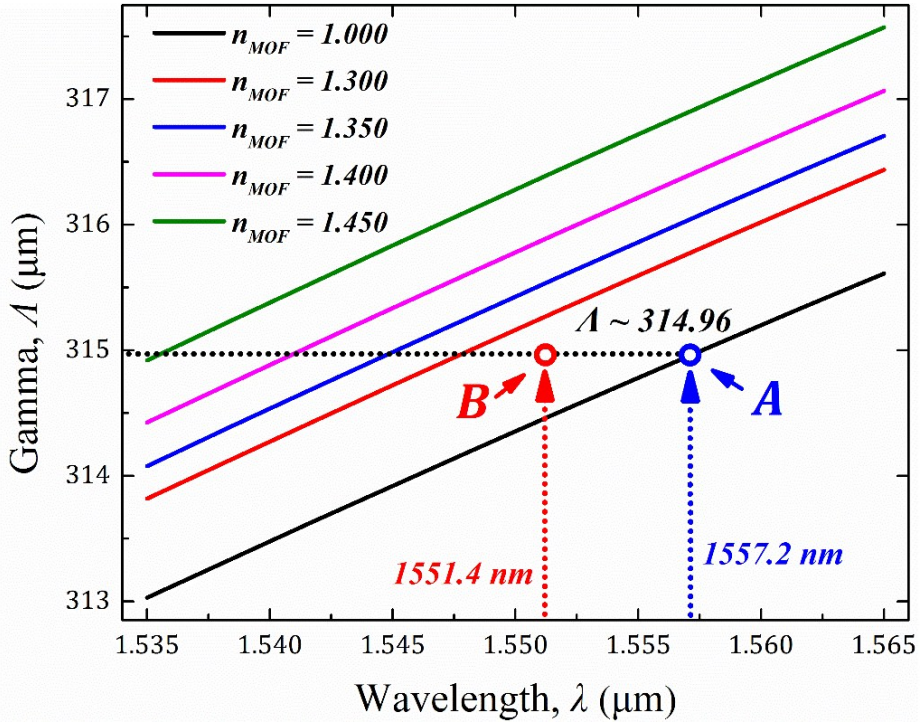

Figure S5. Calculation of the period of LPFG according to the central wavelength shifts in MZI.

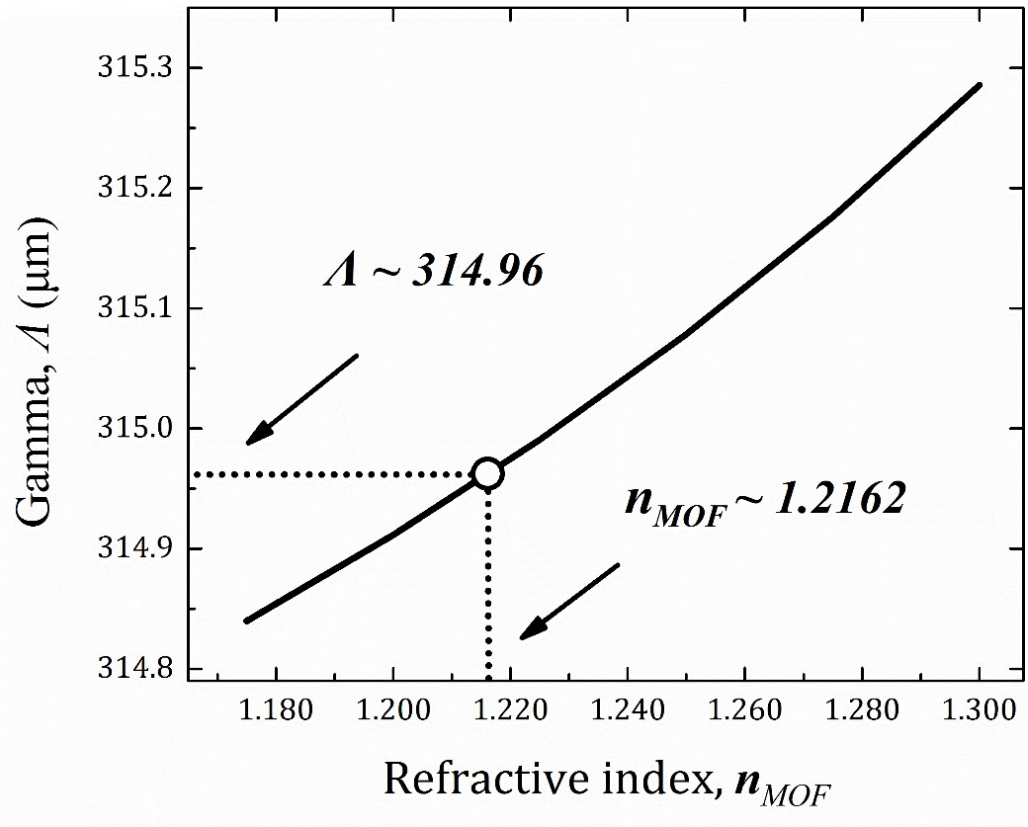

Figure S6. Calculated refractive index of 300 nm-thick ZIF-8.

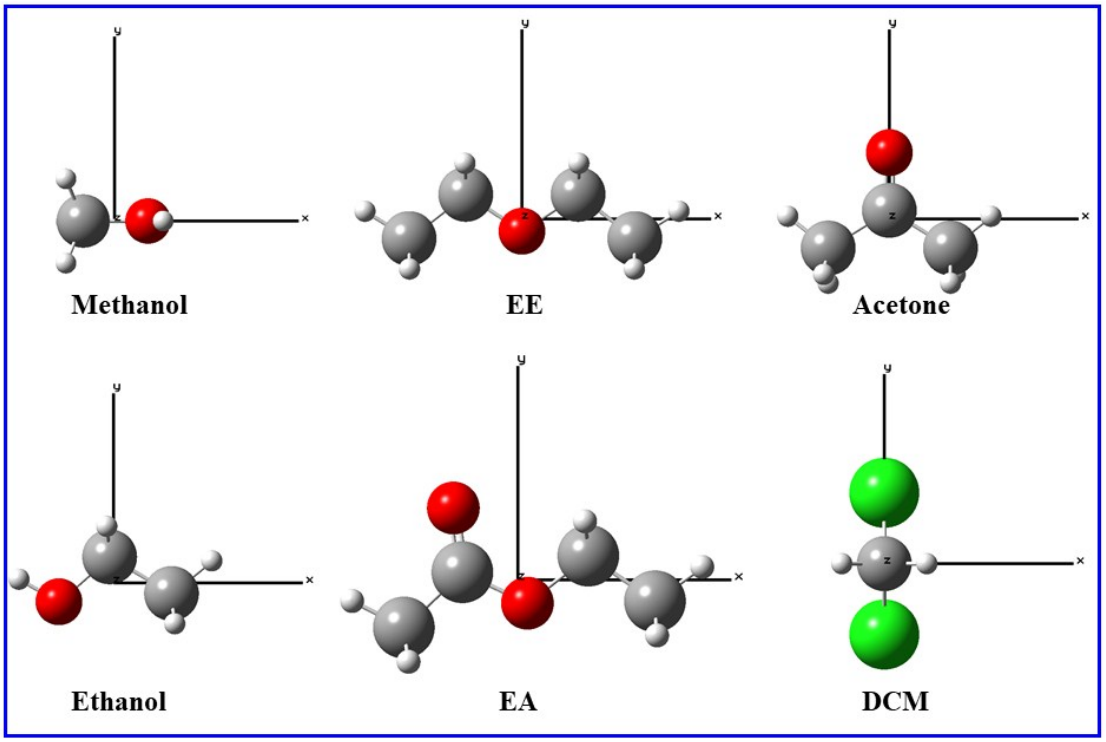

Figure S7. Optimized Guest gas molecules from DFT calculations.

Figure S8. Electric-field distribution of cladding mode LP_{08} after methanol adsorption

Figure S9. Electric-field distribution of cladding mode LP_{08} after ethanol adsorption

Figure S10. Electric-field distribution of cladding mode LP_{08} after acetone adsorption

Figure S11. Electric-field distribution of cladding mode LP_{08} after EE adsorption

Figure S12. Electric-field distribution of cladding mode LP_{08} after EA adsorption

Figure S13. Electric-field distribution of cladding mode LP_{08} after DCM adsorption

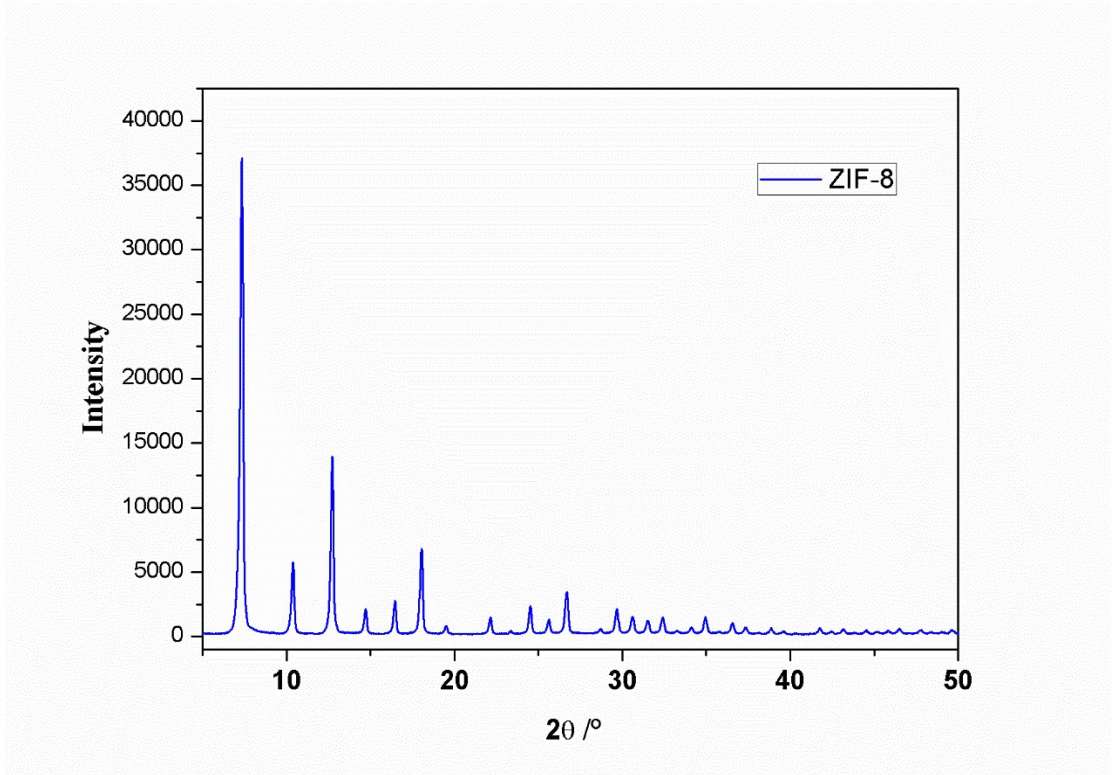

Figure S14. Powder XRD of ZIF-8